

# X-rays from Colliding Stellar Winds: the case of close WR+O binary systems

Svetozar A. Zhekov <sup>\*</sup>

*Space and Sollar-Terrestrial Research Institute, 6 Moskovska str., Sofia-1000, Bulgaria*

## ABSTRACT

We have analysed the X-ray emission from a sample of close WR+O binaries using data from the public *Chandra* and *XMM-Newton* archives. Global spectral fits show that two-temperature plasma is needed to match the X-ray emission from these objects as the hot component ( $kT > 2$  keV) is an important ingredient of the spectral models. In close WR+O binaries, X-rays likely originate in colliding stellar wind (CSW) shocks driven by the massive winds of the binary components. CSW shocks in these objects are expected to be radiative due to the high density of the plasma in the interaction region. Opposite to this, our analysis shows that the CSW shocks in the sample of close WR+O binaries are *adiabatic*. This is possible only if the mass-loss rates of the stellar components in the binary are at least one order of magnitude smaller than the values currently accepted. The most likely explanation for the X-ray properties of close WR+O binaries could be that their winds are two-component flows. The more massive component (dense clumps) play role for the optical/UV emission from these objects, while the smooth rarefied component is a key factor for their X-ray emission.

**Key words:** shock waves - stars: individual: WR46, WR47, WR79, WR139, WR141, WR145, WR148 - stars: Wolf-Rayet - X-rays: stars

## 1 INTRODUCTION

As first proposed by Prilutskii & Usov (1976) and Cherepashchuk (1976), the present concept on the origin of X-rays in massive Wolf-Rayet+O (WR+O) binaries assumes that they arise in colliding-stellar-wind (CSW) shocks resulting from the interaction of the massive winds of the stars in the binary. High wind velocities and high mass-loss rates of WR and O stars suggest that the CSW region will be a luminous X-ray source. Thus, WR+O binaries are expected to be brighter (more luminous) in X-rays than single WR stars and, in fact, this was found in the early surveys of WR stars (Pollock 1987).

It is interesting to note that wide WR+O binaries are among the brightest WR objects in X-rays and their grating spectra with the modern observatories (*Chandra*, *XMM-Newton*) show numerous lines of various ionic species that indicate thermal emission (Skinner et al. 2001; Raassen et al. 2003; Schild et al. 2004; Pollock et al. 2005; Zhekov & Park 2010b). Analyses of these data confirmed that X-rays from CSW shocks is the most probable physical picture for the X-ray emission from wide WR+O binaries (although in some cases the observed picture might be more complex than that; Zhekov & Park 2010a,b).

On the other hand, it is noted from those early X-ray surveys (Pollock 1987) that close WR+O binaries are not as luminous in X-rays as the wide WR+O binaries. This is an important observation since the stellar wind parameters (which in general determine the X-ray emission from CSWs) are practically within the same range for both types of binary systems.

As a possible resolution to this problem, Cherepashchuk (1990) proposed that most of the mass flux in the stellar wind of a WR star is in the form of dense clouds. These clouds penetrate freely the CSW region formed by the continuous component of the winds and they do not contribute to the X-ray emission from the binary. Thus, in a close WR+O binary only small part of the stellar wind gas (the continuous component) plays role for the X-ray emission from the system. However, in a wide WR+O binary the CSW region forms far from the stars where the dense clouds have already expanded and ‘dissolved’ in the continuous component of the wind, thus, the entire mass flux of the stellar wind contributes to the X-ray emission from the binary.

Since the modern X-ray observatories (*Chandra*, *XMM-Newton*) provide us with data of much higher quality (both in sensitivity and spatial resolution) compared to that of previous X-ray missions, we decided to explore the case of CSWs in close WR+O binaries in some detail. This was

<sup>\*</sup> E-mail: szhekov@space.bas.bg

done for a number of such objects that have been observed by *Chandra* and/or *XMM-Newton*. We define the sample of close WR+O binaries in Section 2 and we describe the corresponding X-ray data in Section 3. In Section 4, we present the results from the global spectral models. In Section 5, we discuss our results and we list our conclusions in Section 6.

## 2 THE CSW BINARIES SAMPLE

In the sample of close CSW binaries, we included those objects of known WR+O binaries (van der Hucht 2001; Tables 18 and 19) with orbital period smaller than 20-22 days. We have checked the archives of the modern X-ray observatories (*Chandra* and *XMM-Newton*) for available data on the thus defined sample. Some objects with X-ray detection are not included in our study and we particularly mention the following objects: WR48 (because it is a suggested triple stellar system and its X-ray emission is quite complex; see Sugawara et al. 2008); WR43a (since it is in the core of NGC 3603, thus, the object cannot be resolved); WR101k (it is in the center of the Galaxy and unresolved: being in  $1''.8$  from Sgr A; SIMBAD).

Table 1 presents the list of close CSW binaries considered in this work and summarizes some of their properties.

## 3 X-RAY DATA

Since the studied objects are not very bright in X-rays, we made use of the available data from the Advanced Camera for Imaging Spectroscopy (ACIS-S) on-board *Chandra* and of the data from the European Photon Imaging Camera (EPIC; pn and MOS detectors) on-board *XMM-Newton*.

For the analysis of the ACIS-S data, we extracted the X-ray spectra following procedures in the Science Threads for Imaging Spectroscopy of the CIAO<sup>1</sup> 4.3 data analysis software. The response functions and ancillary response functions for all spectra were generated using the *Chandra* calibration data base CALDB v4.4.2.

For extracting X-ray spectra from the EPIC (pn, MOS) data, we made use of the *XMM-Newton* SAS<sup>2</sup> 10.0.0 data analysis software. The SAS pipeline processing scripts `emproc` and `epproc` were executed to incorporate the most recent calibration files. The data were then filtered for high X-ray background following the instructions in the SAS documentation (e.g., adopting typical threshold rates for high-energy background in pn and MOS: 0.4 and 0.2 cts s<sup>-1</sup>, respectively). The SAS procedures `rmfgen` and `arfgn` were adopted to generate the corresponding response matrix files and ancillary response files for each spectrum. For each data set, the MOS spectra in this analysis are the sum of the spectra from the two MOS detectors.

Table 2 presents the basic information about the X-ray data of the objects in our sample of close CSW binaries. Also, some details on the individual objects are given below.

**WR46.** There is one pointed observation of this object with *XMM-Newton*. The EPIC data are of good quality

(no long background flares), thus, all the spectra, pn and combined MOS, were included in this analysis. This is the object with the shortest binary period in our sample (see Table 1), thus, the EPIC spectra are average (integrated) over the binary period (also, see Appendix A for discussion of the variability issue).

**WR47.** There are three pointed observations of this star in the *XMM-Newton* archive and only two of them (see Table 2) were used in this study since the third one showed considerable high-energy X-ray background rates. Both pn and MOS spectra were included in the current analysis.

**WR139.** There are six pointed observations of WR139 carried on with *XMM-Newton*, and here we used the pn spectra of three of them that have good photon statistics. The basic reason for the lower quality of the rest of the data sets is the high X-ray background which shortens their effective exposure.

**WR141.** There are two data sets in the *XMM-Newton* archive that detect this WR binary at  $\sim 5'.1$  from the optical axis. Unfortunately, due to the high X-ray background rate, only part of the MOS exposure in the second observation could be used in our analysis.

**WR145.** We find one *Chandra* and three *XMM-Newton* archive observations that have detected this WR star respectively at  $\sim 5'.2$  and  $\sim 9'.6$  from the optical axis. The quality of the EPIC data is not high and only the MOS spectra could be used in this analysis.

**WR148.** In the *XMM-Newton* archive, there are two pointed observations of this distant WR binary. Due to high X-ray background, the pn spectrum of the second data set was excluded from our analysis.

**WR79.** We find two *Chandra* and eight *XMM-Newton* archive observations respectively at  $\sim 1'$  and  $\sim 3'$  from the optical axis, but only the former provide useful X-ray spectra of this WR object. The reason is that there are two nearby sources (within  $6''$  from WR79) that cannot be spatially resolved by *XMM-Newton* (see Appendix A for details).

## 4 GLOBAL FITS

Since it is expected that the X-ray emission from the close WR+O binaries originates in the interaction region of their massive winds, a systematic approach to modelling these spectra could be to use a hydrodynamic CSW model. However, the quality of the current data (undispersed CCD spectra with not very good photon statistics for most of the spectra) is not a good basis for carrying on such a modelling in detail. This is why, we decided to use conventional, discrete-temperature plasma, models for the global fits to the X-ray spectra of the objects in our sample. Thus, we adopted the optically thin plasma model *apex* in a recent version (11.3.2) of the XSPEC analysis package (Arnaud 1996). Since the shocked WR gas dominates the X-ray emission from CSWs in WR+O binaries (the mass loss of a WR star is about an order of magnitude higher than of an O star), in the global spectral fits we kept the abundances of the chemical elements fixed to their values typical for the WN and WC stars, correspondingly (van der Hucht et al. 1986). To derive the X-ray absorption towards each object, we used the Morrison & McCammon (1983) cross-sections (model *wabs* in XSPEC). And it is worth noting that we found X-ray

<sup>1</sup> Chandra Interactive Analysis of Observations (CIAO), <http://cxc.harvard.edu/ciao/>

<sup>2</sup> Science Analysis Software (SAS), <http://xmm.esac.esa.int/sas/>

**Table 1.** Properties of the close WR+O binaries

Name	Spectral type	$A_v$ (mag)	Distance (kpc)	Period (days)	$V_\infty$ (km s $^{-1}$ )	$\dot{M}$ ( $M_\odot$ yr $^{-1}$ )	Sources used for $\dot{M}$
WR46	WN3+OB	1.05	4.07	0.329	2450	9.94e-06	2, 3
WR47	WN6+O5	3.96	3.80	6.24	1660	2.30e-05	6, 7, 10, 12
WR139	WN5+O	2.83	1.90	4.21	1600	1.70e-05	1, 4, 5, 8, 10, 11, 12, 13
WR141	WN5+O5	4.10	1.26	21.7	1550	2.48e-05	1, 8, 10
WR145	WN7/WCE+?	—	1.70	22.55	1390	3.68e-05	1, 10
WR148	WN8+B3	2.58	8.28	4.32	1500	3.95e-05	8, 9, 12
WR79	WC7+O5-8	1.54	1.99	8.89	2270	5.59e-05	1, 6, 10, 11, 12

Note – The object name, spectral type, interstellar extinction, distance, orbital period and wind velocity are from the VII-th catalogue of galactic Wolf-Rayet stars (van der Hucht 2001;  $A_v = 1.11A_V$ ) with the following exceptions: (a) the wind velocity for WR47 is the mean value for WN6 stars from Eenens & Williams (1994) and for WR148 is from Nishimaki et al. (2008); (b) the orbital period for WR46 is from Marchenko et al. (2000) and for WR145 is from Muntean et al. (2009); (c) the distance to WR145 is that to Cyg OB2. The mass-loss rates are the mean values for each object as found in the literature with no clumping taken into account. The individual data were scaled correspondingly if derived at values for the distance to the object and/or its stellar wind velocity different from those adopted here. The corresponding references are: (1) Abbott et al. (1986); (2) Crowther et al. (1995); (3) Hamann & Koesterke (1998); (4) Hirv et al. (2006); (5) Kurosawa et al. (2002); (6) Lamontagne et al. (1996) (7) Moffat et al. (1990); (8) Nishimaki et al. (2008); (9) Nugis et al. (1998); (10) Nugis & Lamers (2000); (11) Prinja et al. (1990); (12) St-Louis et al. (1988); (13) St-Louis et al. (1993).

**Table 2.** X-ray Observations

Name	Observation IDs	Binary phase	Detector	Source counts	Rate (cts s $^{-1}$ )	Data		
WR46	0109110101	0.55	pn	3790	6.20e-02	3, 4, 5		
			MOS	2605	3.62e-02			
WR47	0109480101	0.62	pn	1911	4.50e-02	1		
			MOS	1665	3.22e-02			
	0109480401	0.89	pn	1004	2.86e-02			
			MOS	843	1.99e-02			
WR139	0206240201	0.47	pn	1514	0.176	1, 2		
	0206240701	0.55	pn	1723	0.214			
	0206240801	0.81	pn	3744	0.273			
WR141	0404540201	0.02	MOS	734	5.30e-02	5		
WR145	10969	0.33	ACIS-S	757	2.64e-02			
	0165360101	0.00	MOS	297	2.06e-02			
	0165360201	0.09	MOS	366	2.54e-02			
WR148	0165360401	0.18	MOS	361	2.50e-02			
			0405060201	0.99	pn		231	1.11e-02
			MOS	214	7.48e-03			
WR79	0405060301	0.44	MOS	107	8.32e-03			
	5372	0.72	ACIS-S	384	5.04e-03			
	6291	0.23	ACIS-S	203	4.57e-03			

Note – The binary phase for each observation was calculated using the value for  $T_0$  from Pourbaix et al. (2004; The ninth catalogue of spectroscopic binary orbits) except for WR46 (see notes to Table 1). The orbital ‘phase’ for WR145 is with respect of the first in time X-ray observation since no value for  $T_0$  is available in the literature. The moment  $T_0$  (binary phase 0.0) is the time of maximum value of the radial velocity of the WR component in the binary system. The values for the orbital period in Pourbaix et al. (2004) are identical to those in Table 1 except for WR46 and WR145. For these two, we used more recent sources given in the notes to Table 1. The last column gives the references where the corresponding X-ray data have been already discussed in some detail: (1) Bhatt et al. (2010); (2) Faucher et al. (2011); (3) - Gosset et al. (2011a); (4) Hénault-Brunet et al. (2011); (5) Nazé (2009).

absorption higher than that expected from the optical/UV observations. Since the interaction region in close CSW binaries should be located near the massive stars, it is realistic to attribute this extra X-ray absorption to the massive stellar winds of these objects. For sake of simplicity, we assumed that the extra absorption is due to the stellar wind of the WR star in the system because it is considerably more massive than that of its companion.

Thus, the models for our final global spectral fits consisted of the following components. An absorption component due to the interstellar matter towards the studied object (model *wabs* in XSPEC). The value of the neutral hydrogen column density was kept fixed to that based on the optical/UV observations (e.g.  $A_v$  in Table 1) through the Gorenstein (1975) conversion ( $N_H = 2.22 \times 10^{21} A_V \text{ cm}^{-2}$ ). Anticipating the discussion of the derived results, we note

that our conclusions from this study do not change if we use a more recent conversion (Vuong et al. 2003; Getman et al. 2005;  $N_H = 1.6 - 1.7 \times 10^{21} \text{A}_V \text{ cm}^{-2}$ ). Emission components are represented with discrete-temperature optically-thin plasma models (*apec* in XSPEC) with individual ‘wind’ absorption for each plasma component. The emission and ‘wind’ absorption components had the same abundances. We recall that in the framework of the CSW picture, the discrete-temperature models represent qualitatively the temperature stratification of the interaction region (see §5.2 in Zhekov 2007). We note that there are no objects in our sample of close CSW binaries that have elliptical orbits. This means that the amount of hot gas in the interaction region remains the same over an orbital period. So, for each object that had multi-phase observations, we adopted the same model normalization for the corresponding plasma component. This is equivalent to a non-variable emission measure with the orbital phase that is there is no variation in the intrinsic X-ray emission. We thus attribute a possible X-ray variability to the variable X-ray absorption with the orbital phase.

One-temperature model was successful for fitting the X-ray spectrum of WR141. We found that two-temperature models gave adequate global fits for the X-ray emission from all other WN and WC stars in the sample but WR46. For the latter, we needed a three-temperature model. We note that the two-temperature one gave a statistically acceptable result but it was not able to match all the spectral details in the spectrum: e.g., it produced almost none emission for the Si XIII line complex at  $\sim 1.85 \text{ keV}$  and variable silicon abundances could not fix this problem. It is our understanding that a more complex model was needed in this case due to the good photon statistics of the WR46 spectra (the best quality data in our sample). Also, we had no data on the interstellar absorption towards WR145, we thus fitted for the X-ray absorption in the global spectral fits for this object.

Figure 1 and Table 3 present the results from the global fits to the X-ray spectra of our sample of close WR+O binaries. We see that the quality of the fits is acceptable but we note that in many of the studied cases the formal quality of the fit ( $\chi^2/\text{dof}$ ) is good likely due to the low photon statistics. Nevertheless, we note that the fit results firmly establish that a considerable amount of hot-temperature plasma ( $\text{kT} > 2 \text{ keV}$ ) is present in the studied objects. The ‘canonical’ WN and WC abundances adopted here (van der Hucht et al. 1986) seem to be an adequate approximation to the actual abundances in the studied objects. Although, a by-product from these fits in this respect is worth mentioning. Namely, as seen from Fig. 1 the SXV line complex at  $\sim 2.45 \text{ keV}$  is not well matched by the current model. Our attempts to solve this problem by adding an additional temperature component were not successful. The only way to match the SXV ‘bump’ in the spectra was to adopt a variable sulfur abundance. Interestingly, the values for the S abundance derived from all fits are not widely spread but ‘cluster’ around a factor of three increase with respect to the one in the ‘canonical’ WN and WC abundances. More specifically, the average sulfur abundance from all data sets is  $2.97 \pm 0.33$  (where the error is the error of the mean and not the variance). We note that the sulfur value in the van der Hucht et al. (1986) WN and WC abundances is based on the cosmic mass fraction (see the footnote to their

Table 1), thus, we get an indication from the current analysis that the sulfur abundance in the ‘canonical’ WN and WC sets of abundances may need be increased by a factor of three.

In the next section, we will discuss the global fit results in the framework of the CSW picture.

## 5 DISCUSSION

Although our sample of close WR+O binaries is limited, the adopted uniform way of analysing the X-ray emission from the studied objects provides useful pieces of information to check the global consistency of the colliding stellar wind picture in such objects. We note that our spectral analysis adopted simplified models: those of discrete-temperature optically-thin plasma (§ 4). This means that the X-ray emitting plasma is in collisional ionization equilibrium (CIE), that is the non-equilibrium ionization (NEI) effects do not affect its emission. Also, the electron and ion temperatures are equal. We can use the corresponding characteristic plasma timescales to check validity of these assumptions in the case of close WR+O binaries.

For this purpose, two dimensionless parameters have been introduced  $\Gamma_{eq} = \tau/\tau_{eq}$  (Zhekov & Skinner 2000) and  $\Gamma_{NEI} = \tau/\tau_{NEI}$  (Zhekov 2007), where  $\tau$  is the timescale of the gasdynamics,  $\tau_{eq}$  is the electron-ion temperature equalization time and  $\tau_{NEI}$  is the representative NEI timescale. We recall that the electron and ion temperatures are different if  $\Gamma_{eq} \leq 1$  but their difference can be neglected if  $\Gamma_{eq} \gg 1$ . Similarly, the NEI effects must be taken into account if  $\Gamma_{NEI} \leq 1$  but can be neglected if  $\Gamma_{NEI} \gg 1$ .

For a total mass of the WR+O systems of  $30-40 M_\odot$ , we can use the Kepler’s third law ( $a = 2.928 \times 10^{11} P_d^{2/3} [M/M_\odot]^{1/3} \text{ cm}$ ;  $P_d$  is the orbital period in days (Table 1);  $M$  is the total mass) to estimate the typical lengthscale for the gasdynamic problem (e.g., the binary separation). Then the stellar wind parameters from Table 1 ( $M, V_\infty$ ) along with eq.(1) in Zhekov & Skinner (2000) and eq.(1) in Zhekov (2007) show that, first, the plasma in the CSW shock in the close WR+O binaries considered here has equal electron and ion temperatures ( $\Gamma_{eq} \gg 1$ ). Second, the NEI effects are not important in these objects ( $\Gamma_{NEI} \gg 1$ ). All this makes us confident that the adopted spectral models in this study were adequate to the physical conditions of the X-ray emitting plasma in close WR+O binaries.

On the other hand, when fitting the total (‘integrated’) X-ray emission from temperature stratified plasmas (e.g., present in the interaction region in CSW binaries) with discrete-temperature models, we can expect that the derived plasma temperatures will not be higher than the maximum one in the X-ray emitting region. We note that for a strong shock (with adiabatic index  $\gamma = 5/3$ ) in helium-dominated plasma (mean molecular weight per particle  $\mu = 4/3$ ) the postshock temperature is  $\text{kT} = 2.608 (V_{sh}/1000 \text{ km s}^{-1})^2 \text{ keV}$ , where  $V_{sh}$  is the shock velocity, and the maximum shock velocity is equal to the stellar wind velocity ( $V_{sh} = V_\infty$ ) in the framework of CSW model. We thus see from Tables 1 and 3 that the deduced plasma temperatures in our sample of close WR+O binaries are qualitatively consistent with the adopted physical picture. Namely, all of them are lower than the maximum possible

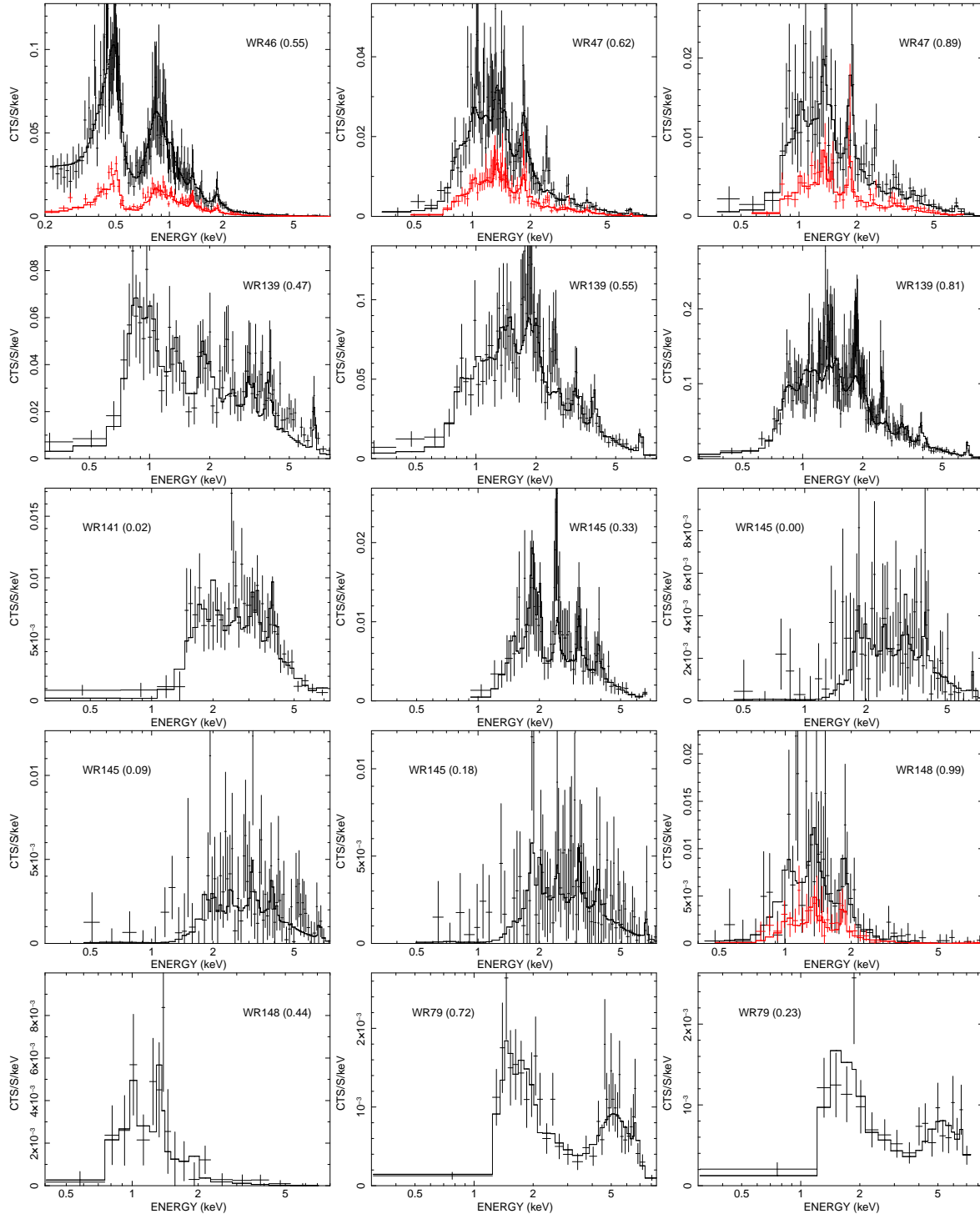


**Figure 1.** The background-subtracted spectra overlaid with the best-fitting model. Each panel is marked by the name of the object and the binary phase in parentheses (see Tables 2 and 3). The spectra are re-binned to have a minimum of 10-20 counts per bin. In the panels with two different spectra in the same data set, the upper and lower (in red) curves are for the pn and MOS spectrum, respectively.

plasma temperature in the interaction region of these CSW objects.

Also, in the CSW picture the hotter plasma is located near the line connecting the two stellar components in the binary system, that is in the denser part of the stellar winds. Thus, we can expect that the higher-temperature component of the discrete-temperature models will suffer higher ‘wind’

absorption. As seen from Table 3, this is in general found in the spectral fits to the X-ray emission from the close WR+O binaries in our sample (although there are some exceptions but likely due to the poor photon statistics).

It then seems conclusive that the X-ray emission from the close WR+O binaries considered in this study is qualitatively consistent with the physical picture where X-rays

**Table 3.** Global Spectral Model Results

Name	Phase <sup>(a)</sup>	$\chi^2/\text{dof}$	$N_{H, ISM}$ <sup>(b)</sup>	$N_{He, 1}$ <sup>(c)</sup>	$kT_1$ <sup>(d)</sup>	$EM_1$ <sup>(e)</sup>	$N_{He, 2}$ <sup>(c)</sup>	$kT_2$ <sup>(d)</sup>	$EM_2$ <sup>(e)</sup>	$F_X$ <sup>(f)</sup>
WR46	0.55	231/255	2.10	$0.002^{+0.34}_{-0.002}$	$0.15^{+0.01}_{-0.01}$	$5.55^{+31.5}_{-0.27}$	$0.35^{+0.09}_{-0.09}$ $0.44^{+0.72}_{-0.44}$	$0.57^{+0.02}_{-0.02}$ $3.43^{+1.07}_{-0.28}$	$3.75^{+0.83}_{-0.65}$ $3.28^{+0.52}_{-0.61}$	1.20 (3.00)
WR47	0.62 0.89	244/295	7.92	$0.53^{+0.08}_{-0.11}$ $0.80^{+0.16}_{-0.10}$	$0.59^{+0.03}_{-0.03}$	$12.3^{+1.3}_{-1.2}$	$0.00^{+0.21}_{-0.00}$ $4.33^{+0.78}_{-0.66}$	$4.02^{+0.34}_{-0.33}$	$8.05^{+0.41}_{-0.38}$	2.27 (8.02) 1.70 (8.02)
WR139	0.47 0.55 0.81	362/335	5.86	$0.23^{+0.16}_{-0.16}$ $0.43^{+0.12}_{-0.15}$ $0.10^{+0.09}_{-0.10}$	$0.58^{+0.04}_{-0.03}$	$3.66^{+0.60}_{-0.35}$	$6.11^{+0.63}_{-0.58}$ $2.07^{+0.29}_{-0.26}$ $1.00^{+0.19}_{-0.18}$	$3.08^{+0.13}_{-0.13}$	$17.8^{+0.71}_{-0.62}$	9.40 (27.3) 11.8 (27.3) 13.4 (27.3)
WR141	0.02	35/39	8.20	$4.40^{+0.59}_{-0.53}$	$3.40^{+0.43}_{-0.30}$	$6.82^{+0.75}_{-0.68}$	...	...	...	8.49 (19.1)
WR145	0.33 0.00 0.09 0.18	180/278	$35.4^{+3.5}_{-2.2}$ $47.5^{+8.9}_{-6.9}$ $57.5^{+8.4}_{-6.9}$ $47.5^{+7.5}_{-5.9}$	0.0 0.0 0.0 0.0	$0.99^{+0.14}_{-0.12}$	$16.5^{+3.5}_{-4.5}$	0.0 0.0 0.0 0.0	$4.75^{+1.46}_{-1.00}$	$4.90^{+1.27}_{-1.02}$	6.32 (39.7) 4.80 (39.7) 4.59 (39.7) 5.10 (39.7)
WR148	0.99 0.44	54/101	5.16	$1.98^{+1.20}_{-0.73}$ $1.03^{+0.49}_{-0.50}$	$0.40^{+0.18}_{-0.11}$	$44.5^{+123.}_{-26.5}$	$1.69^{+1.83}_{-1.69}$ $10.1^{+52.4}_{-6.43}$	$1.03^{+1.11}_{-0.33}$	$9.73^{+12.1}_{-7.64}$	0.255 (4.14) 0.249 (4.14)
WR79	0.72 0.23	40/49	3.08	$0.09^{+0.01}_{-0.01}$ $0.09^{+0.02}_{-0.02}$	$1.27^{+0.48}_{-0.20}$	$0.09^{+0.02}_{-0.01}$	$3.92^{+1.26}_{-0.64}$ $4.21^{+1.40}_{-0.78}$	$2.38^{+0.98}_{-0.78}$	$2.92^{+4.69}_{-1.35}$	1.80 (33.6) 1.70 (33.6)

Note – Fit results from the two-temperature optically-thin plasma model with individual wind absorption for each component. A three-temperature plasma model was used only in the case of WR46: parameters of the third component are given in the second line for this object. The uncertainties are  $1\sigma$  errors from the fit.

<sup>(a)</sup>The binary phase for each observation from Table 2.

<sup>(b)</sup>The interstellar absorption column density in units of  $10^{21} \text{ cm}^{-2}$ .

<sup>(c)</sup>The helium-dominated wind absorption column density in units of  $10^{21} \text{ cm}^{-2}$ .

<sup>(d)</sup>The plasma temperature is in keV.

<sup>(e)</sup>The emission measure ( $EM = \int n_e n_{He} dV$ ) in units of  $10^{54} \text{ cm}^{-3}$  at the distance for each object from Table 1.

<sup>(f)</sup>The observed flux (0.5 - 10 keV) followed in parentheses by the unabsorbed value. The units are  $10^{-13} \text{ erg cm}^{-2} \text{ s}^{-1}$ .

arise in hot temperature-stratified plasmas behind colliding stellar wind shocks. But, an interesting issue is worth discussing as well, namely, the total X-ray energetics (luminosity) of CSWs in close binaries which is directly related to whether the CSW shocks are radiative, adiabatic etc.

We can use the dimensionless parameter  $\chi = \tau_{cool}/\tau$  introduced by Stevens et al. (1992) to estimate the importance of radiative losses behind the CSW shocks in the WR+O binaries of our sample. We recall that  $\tau_{cool}$  and  $\tau$  are the characteristic cooling time of the shocked plasma and the timescale of the gasdynamics, respectively. Then from the data in Table 1 and eq.(8) in Stevens et al. (1992), we see that the radiative cooling should have an important effect on the physics of CSWs in the close WR+O binaries studied here ( $\chi < 1$ ). This means that only numerical hydrodynamic modelling of the interaction region must be used to confront theory and observations. However, we can perform a qualitative check on the X-ray energetics, as mentioned above, by considering two extremes: (a) highly radiative and (b) adiabatic CSW shocks.

In the case of radiative shocks, we have an upper limit on the available energy (luminosity) that can be converted into X-ray emission: no more energy is emitted than the energy flux crossing the shock front per unit area. For the maximum X-ray luminosity, we have  $L_X = \frac{1}{2} \int \rho V_{wind,\perp}^3 dS$  ( $\rho$  is the density of the wind in front of the shock;  $V_{wind,\perp}$  is the wind velocity component perpendicular to the shock front;  $S$  is the shock surface). In the case of CSWs, the integration is over the entire CSW ‘cone’ and although its shape varies from one object to another we can expect that a rela-

tion  $L_X \propto L_{wind}$  might hold in general for highly radiative CSWs ( $L_{wind} = \frac{1}{2} \dot{M} V_\infty^2$  is the stellar wind luminosity).

On the other hand, in the case of adiabatic CSWs there exists a scaling law for the CSW X-ray luminosity with the mass-loss rate ( $\dot{M}$ ), wind velocity ( $V_\infty$ ) and binary separation ( $a$ ):  $L_X \propto \dot{M}^2 V_\infty^{-3} a^{-1}$  (Luo et al. 1990; Myasnikov & Zhekov 1993). So, using the third Kepler’s law we can write:  $L_X \propto C_{CSW}$  by introducing  $C_{CSW} = (\dot{M}/10^{-5} M_\odot \text{ yr}^{-1})^2 (V_\infty/1000 \text{ km s}^{-1})^{-3} P_d^{-2/3}$  as a ‘colliding stellar wind’ parameter.

Figure 2 presents two plots: the X-ray vs. the wind luminosity and the X-ray luminosity vs. the CSW parameter for the objects in our WR+O binaries sample (the unabsorbed fluxes from Table 3 are used for calculating the X-ray luminosity). We see that there is no correlation for the former while the X-ray luminosity clearly correlates with the CSW parameter. Interestingly, the derived proportionality between  $\log L_X$  and  $\log C_{CSW}$  is  $1.05 \pm 0.09$  (the error is  $1\sigma$  error from the fit), thus,  $L_X \propto C_{CSW}^{1.05 \pm 0.09}$ . All this is quite surprising since it means that the CSW shocks in close WR+O binaries are more likely adiabatic rather than being strongly radiative. We note again that our sample of studied objects is limited but nevertheless the results in Fig. 2 are very interesting and we will discuss them in some detail.

It is worth noting another result from Fig. 2 that favours the case of adiabatic CSWs in the close WR+O binaries in our sample. Namely, the low efficiency of converting the wind luminosity into X-ray emission:  $L_X/L_{wind} \sim 10^{-4} - 10^{-5}$ . Of course, this ratio cannot be very close to unity because the CSW shock cone occupies only part of the ‘sky’ of the

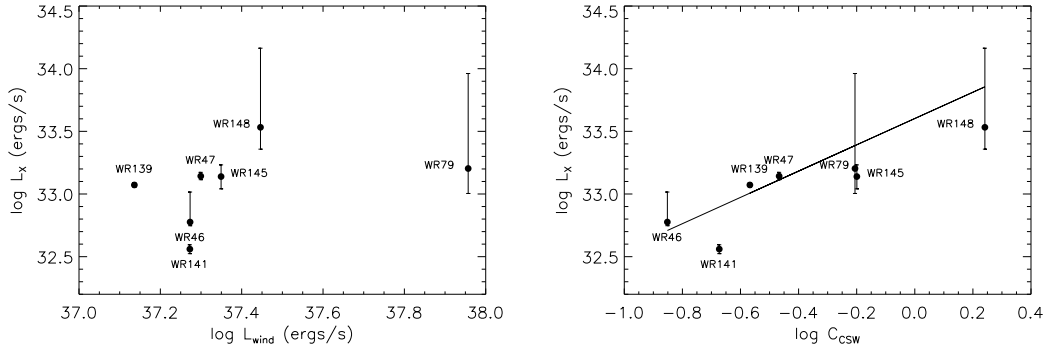


**Figure 2.** *Left panel:* X-ray ( $L_X$ ) vs. wind luminosity ( $L_{wind} = \frac{1}{2}\dot{M}V_\infty^2$ ) for the sample of close CSW binaries. *Right panel:* X-ray luminosity vs. the CSW parameter,  $C_{CSW} = (\dot{M}/10^{-5} M_\odot \text{ yr}^{-1})^2 (V_\infty/1000 \text{ km s}^{-1})^{-3} P_d^{-2/3}$ . The slope of the solid line is  $1.05 \pm 0.09$ . The X-ray luminosity is calculated for the corresponding distance to each object (Table 1). The error bars on  $L_X$  are internal only and do not take into account those on distance to the objects.

WR star (the shocked WR wind dominates the X-ray emission from the interaction region). But, it seems unlikely to explain such a low value of  $L_X/L_{wind}$  only by geometry effects and some other explanation is needed. Moreover, by its very definition the term ‘radiative shocks’ means that high percentage of the energy influx is radiated away (mostly in X-rays for fast shocks), while the opposite is valid for ‘adiabatic shocks’. Figure 3 shows the result from our numerical integration for the maximum possible X-ray luminosity,  $L_X = \frac{1}{2} \int \rho V_{wind,\perp}^3 dS$ , in the case of highly radiative CSW shocks. In such a case, the interaction region ‘collapses’ and its shape coincides with that of the contact discontinuity between the shocked WR and O star winds. We adopted the Canto et al. (1996) solution for the shape of the CSW ‘cone’. We see that the theoretical  $L_X/L_{wind}$  values are considerably higher than those observed. Thus, the relatively low values for the X-ray luminosity, with respect to the wind luminosity of the more massive star in the binary, do support the conclusion that the CSWs in our sample of close WR+O binaries are *adiabatic*.

But, adiabatic CSW shocks are possible in this case *only* if the mass-loss rate of the stellar winds in the binaries is considerably smaller, e.g. at least by an order of magnitude, than the values listed in Table 1 (we note that in such a case the actual values of the CSW parameter will be smaller and the plot in the right panel of Fig. 2 will be shifted to the left in the x-axis; a detailed analysis in that case is needed: see discussion below). In other words, our analysis of the X-ray emission from close WR+O binaries finds an indication of considerable clumping in the winds of these massive stars. It then seems plausible to propose that the stellar wind of a massive WR (O) star is likely a two-component flow: a rarefied continuous component with low mass-loss rate and a ‘discrete’ component consisting of numerous dense clumps. The first component forms the CSW interaction region, thus, it plays role for the X-ray emission from close WR+O binaries while the second one dominates their optical/UV spectra. We note that in the last two decades the physical picture of clumpy stellar winds in the hot massive stars gathered observational evidence and has become a standard ingredient in the analysis of the optical, UV and infrared spectra of these objects (see Puls et al. 2008 for a recent review on the

matter). Here from the analysis of X-ray spectra of close WR+O binaries, we find additional evidence that the stellar wind in massive stars is clumpy (highly inhomogeneous) on a lengthscale at least of the order of the binary separation (approximately the size of the CSW region). It is worth noting though that we need more detailed knowledge, both observational and theoretical, in order to build a coherent physical picture of clumpy stellar winds in massive stars. For example, what is the origin of the clumps; what is the distribution of clumps by their size; what is the clump evolution with the distance from the star; do the homogeneous component of the wind and the clumps share the same bulk velocity; thus, what is the efficiency of the radiative force that drives both of them; do both components of the stellar wind reach terminal wind velocity in front of the interaction region; does radiative braking play an important role for this complex wind structure?

An interesting issue in this respect is about the fate of the dense clumps when interacting with the CSW region of the rarefied homogeneous components of the stellar winds in close WR+O binaries. Cherepashchuk (1990) proposed a qualitative picture where the dense clumps pass freely through the interaction region and part of them are decelerated in the O-star photosphere where their X-rays are transformed into optical emission. On the other hand, Pittard (2007) carried hydrodynamical simulations of a CSW binary with clumpy winds that showed efficient destruction of clumps while interacting with the CSW shocks. As a result, the average density in the interaction region increases and is similar to the case of smooth winds with the higher mass-loss rate. We have to keep in mind that these simulations were suitable for wide CSW binaries and specifically for the stellar wind and binary parameters of WR140 (see Pittard 2007 for details) and the reality might be quite different in close CSW binaries. Namely, the clumps are likely smaller closer to the base of the stellar wind, they may have much larger density contrast with respect to the smooth component etc. Also, if the clumps are destroyed in the CSW region in close WR+O binaries, then these objects would have been much more luminous in X-rays than deduced from observations. Thus, it seems plausible to assume that the dense clumps of the stellar winds ‘survive’ while crossing the CSW region in

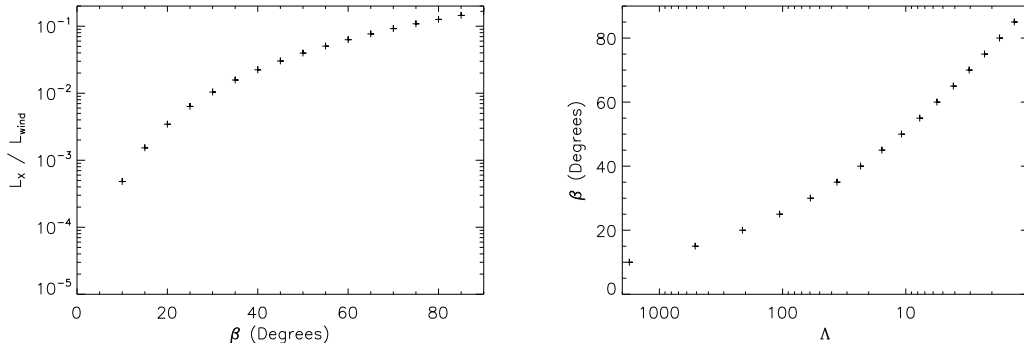


**Figure 3.** *Left panel:* the ratio of the maximum possible X-ray luminosity ( $L_X$ ) to the wind luminosity ( $L_{wind} = \frac{1}{2}\dot{M}V_\infty^2$ ) for different values of the half-opening angle ( $\beta$ ) of the CSW ‘cone’ in the case of highly radiative CSW shocks in binary system. *Right panel:* dependence of the half-opening angle ( $\beta$ ) on the ratio of the ram pressure of the stellar winds in the binary system ( $\Lambda = \dot{M}_{WR}V_{WR}/\dot{M}_OV_O$ , where  $\dot{M}_{WR}, V_{WR}, \dot{M}_O, V_O$  are the wind parameters, mass loss rate and wind velocity, of the WR and O star, respectively).

close WR+O binaries. It is difficult to describe what could be the possible observational evidences from the interaction of these dense clumps with the CSW region since they depend on such ‘hard-to-guess’ details as those mentioned at the end of the previous paragraph.

We thus believe that future X-ray observations with much better photon statistics might be very helpful in this respect. Results from such observations must be considered in conjunction with those from the optical/UV spectral domain to build a self-consistent physical picture of the stellar winds in massive stars. Such a global analysis may reveal that the smooth component has very little or no contribution to the optical/UV emission of a massive star and X-ray observations could be the only tool to reveal its presence and physical properties. It should also take into account that massive O stars are X-ray sources themselves (for a recent review see Güdel & Nazé 2009). We just note that their emission is rather ‘soft’ with plasma temperatures below 1 keV (e.g., Wojdowski & Schulz 2005; Zhekov & Palla 2007; see also Sections 4.1.3 and 4.3 in the review paper of Güdel & Nazé 2009), opposite to what is found in close WR+O binaries (e.g., Table 3). On the other hand, the issue of the intrinsic contribution of the WR star to the total X-ray emission from the binary might still bear a lot of uncertainties.

Pointed observations with modern X-ray observatories (*Chandra*; *XMM-Newton*) of a few presumably single WC stars resulted only in non-detections (Oskinova et al. 2003; Skinner et al. 2006). Could it be that all single WC stars are X-ray quiet? In such a case, there will be no contribution from a WC star to the total X-ray emission from a WR+O binary system.

In contrast to this, the Skinner et al. (2010) analysis of the X-ray spectra of a small sample of presumably single WN stars showed that these objects emit X-rays that arise from an admixture of cool ( $kT < 1$  keV) and hot ( $kT > 2$  keV) plasma. Presence of hot plasma ( $kT > 2$  keV) makes them similar to the CSW binaries studied here and distinct from the single O stars. *So, could it be that these WN stars are not single but binaries instead?* However, there are some differences in the X-ray characteristics between the single WN

stars and the close WR+O binaries in our sample. Namely, the latter are X-ray more luminous with a minimum value of  $\log L_X \approx 32.5$  erg s $^{-1}$  (Fig. 2) while most of the X-ray detected presumably single WN stars have luminosities below this figure (see Fig. 10 in Skinner et al. 2010). Also, there is indication that the  $L_X \propto L_{wind}$  relation holds for single WNs while this is not the case for close WR+O binaries (compare Fig. 10 in Skinner et al. 2010 with the left panel in Fig. 2 here). Since the X-ray production mechanism in single WN stars has not been identified yet, one possibility is that those of them detected in X-rays are in fact WR binaries with a normal (non-degenerate) companion (see discussion in § 4.4 in Skinner et al. 2010) which may also explain the  $L_X \propto L_{wind}$  trend for them (see § 7.2 in Zhekov & Park 2010b). And we emphasize again that more X-ray data with good quality are needed and the global analysis as that mentioned above will help us better understand the physical picture in the stellar winds of hot massive stars.

Finally, the object with the shortest period in our sample, WR46, deserves a few more comments. This object has a very complex variability pattern in the optical, UV and may be X-rays (e.g., Marchenko et al. 2000; Gosset et al. 2011a; Hénault-Brunet et al. 2011; but see also Appendix A here). Gosset et al. (2011a) proposed that its hard X-ray emission may arise in CSW shocks. Hénault-Brunet et al. (2011) argued for non-radial pulsations as the most likely scenario to explain its characteristics and they even drew analogy between WR46 and  $\zeta$  Pup (a massive presumably single O star) in this respect. Based on the results presented here (e.g., high plasma temperatures) and since the X-ray variability pattern is not well established (see Appendix A), we believe that the physical picture of CSWs in a short-period WR+O binary is a more likely explanation for the X-ray properties of WR46.

## 6 CONCLUSIONS

Using data from the *Chandra* and *XMM-Newton* public archives, we have analysed the X-ray emission from a small sample of close WR+O binaries. In such objects, X-rays likely originate in colliding stellar wind shocks driven by the



massive winds of the binary components. The main results and conclusions from our analysis are as follows.

(1) Global spectral fits show that two-temperature plasma is needed to match the X-ray emission from these objects as the hot component ( $kT > 2$  keV) is an important ingredient of the spectral models.

(2) In general, CSW shocks in close binaries are expected to be radiative due to the high density of the plasma in the interaction region and the X-ray emission is dominated by that of the shocked WR wind. Thus, a correlation between the X-ray luminosity from these objects and the mechanical luminosity of the WR wind should exist:  $L_X \propto L_{wind}$ . Interestingly, we do not find such a correlation for the objects studied here.

(3) Our analysis shows that a correlation between the X-ray luminosity and the so called CSW parameter (see § 5) does hold. This means that CSWs in close WR+O binaries must be adiabatic and this is possible only if the mass-loss rates of the hot stars in these objects are at least one order of magnitude smaller than the values currently accepted.

(4) The most likely explanation for the X-ray properties of close WR+O binaries could be that their winds are two-component flows. The more massive component (dense clumps) play role for the optical/UV emission from these objects. However, the smooth rarefied component is a key factor for their X-ray emission. We believe that global analysis (modelling) of optical, UV, X-ray emission from close WR+O binaries will help us build a self-consistent physical picture of the stellar winds and the close circumstellar environment in these objects.

(5) To further check the results presented here, similar analysis should be applied to close O+O binaries since they are evolutionary progenitors of the WR+O binaries. The work by De Becker et al. (2004) is an example for the relevance of such a proposition. Their study of the X-ray emission from HD159176 (an O+O system with a 3.367-day period) showed that the CSW model overestimates the observed X-ray luminosity for the standard wind parameters.

## 7 ACKNOWLEDGMENTS

The author acknowledges financial support from Bulgarian National Science Fund grant DO-02-85. This research has made use of the NASA's Astrophysics Data System, and the SIMBAD astronomical data base, operated by CDS at Strasbourg, France. Also, the author thanks the referee Eric Gosset for valuable comments and suggestions.

## REFERENCES

- Abbott D.C., Biegging J.H., Churchwell E., Torres A.V. 1986, *ApJ*, 303, 239
- Arnaud, K.A. 1996, in Jacoby G., Barnes, J. eds., *ASP Conf. Ser. Vol. 101, Astronomical Data Analysis Software and Systems*, Astron. Soc. Pac., San Francisco, 17
- Bhatt, H., Pandey, J.C., Kumar, B., Singh, K.P., & Sagar, R. 2010, *MNRAS*, 402, 1767
- Canto, J., Raga, A.C., & Wilkin, F.P. 1996, *ApJ*, 469, 729
- Cherepashchuk, A.M. 1976, *Soviet Astronomy Letters*, 2, 138
- Cherepashchuk, A.M. 1990, *Soviet Astronomy*, 34, 481
- Crowther, P.A., Smith, L.J., & Hillier, D.J. 1995, *A&A*, 302, 457
- De Becker, M., Rauw, G., Pittard, J.M., Antokhin, I.I., Stevens, I.R., Gosset, E., & Owocki, S.P. 2004, *A&A*, 416, 221
- Eenens, P.R.J., & Williams, P.M. 1994, *MNRAS*, 260, 1082
- Fauchez, T., De Becker, M., & Nazé, Y. 2011, *Bulletin de la Société Royale des Sciences de Liège*, 80, 673
- Getman, K.V., Feigelson, E.D., Grosso, N., McCaughrean, M.J., Micela, G., Broos, P., Garmire, G., & Townsley, L. 2005, *ApJS*, 160, 363
- Gorenstein, P. 1975, *ApJ*, 198, 95
- Gosset, E., De Becker, M., Nazé, Y., Carpano, S., Rauw, G., Antokhin, I.I., Vreux, J.-M., & Pollock, A.M.T. 2011, *A&A*, 527, A66
- Gosset, E., Sana, H., Rauw, G., & Nazé, Y. 2011, *Bulletin de la Société Royale des Sciences de Liège*, 80, 683
- Güdel, M., & Nazé, Y. 2009, *The Astronomy and Astrophysics Review*, 17, 309
- Hamann, W.-R., & Koesterke, L. 1998, *A&A*, 333, 251
- Hénault-Brunet, V., St-Louis, N., Marchenko, S.V., Pollock, A.M.T., Carpano, S., & Talavera, A. 2011, *ApJ*, 735, 13
- Hirv, A., Annuk, K., Eenmaë, T., Liimets, T., Pelt, J., Puss, A., & Tempel, M. 2006, *Baltic Astronomy*, 15, 405
- Kurosawa, R., Hillier, D.J., & Pittard, J.M., 2002, *A&A*, 388, 957
- Lamontagne, R., Moffat, A.F.J., Drissen, L., Robert, C., & Matthews, J.M. 1996, *AJ*, 112, 2227
- Luo, D., McCray R., & Mac Low, M.-M. 1990, *ApJ*, 362, 267
- Marchenko, S.V., Arias, J., Barbá, R., Balona, L., Moffat, A.F.J., Niemela, V.S., Shara, M.M., & Sterken, C. 2000, *AJ*, 120, 2001
- Moffat, A.F.J. et al. 1990, *ApJ*, 350, 767
- Morrison, R., & McCammon, D. 1983, *ApJ*, 270, 119
- Muntean, V., Moffat, A.F.J., Chene, A.N., & De La Chevrotiere, A. 2009, *MNRAS*, 399, 1977
- Myasnikov, A.V. & Zhekov, S.A. 1993, *MNRAS*, 260, 221
- Nazé, Y. 2009, *A&A*, 506, 1055
- Nishimaki, Y., Yamamuro, T., Motohara, K., Miyata, T., & Tanaka, M. 2008, *PASJ*, 60, 191
- Nugis, T., Crowther, P.A., & Willis, A.J. 1998, *A&A*, 333, 956
- Nugis, T., & Lamers, H.J.G.L.M. 2000, *A&A*, 360, 227
- Oskinova, L.M., Ignace, R., Hamann, W.-R., Pollock, A.M.T., & Brown, J.C. 2003, *A&A*, 402, 755
- Pittard, J.M. 2007, *ApJ*, 660, L141
- Pollock, A.M.T. 1987, *ApJ*, 320, 283
- Pollock, A.M.T., Corcoran, M.F., Stevens, I.R., & Williams, P.M. 2005, *ApJ*, 629, 482
- Pourbaix, D. et al. 2004, *A&A*, 424, 727
- Prilutskii, O.F & Usov, V.V. 1976, *Soviet Astronomy*, 20, 2
- Prinja, R.K., Barlow, M.J., & Howarth, I.D. 1990, *ApJ*, 361, 607
- Puls, J., Vink, J.S., & Najarro, F. 2008, *The Astronomy and Astrophysics Review*, 16, 209
- Raassen, A.J.J., van der Hucht, K.A., Mewe, R., Antokhin, I.I., Rauw, G., Vreux, J.-M., Schmutz, W., & Güdel, M. 2003, *A&A*, 402, 653

- Schild, H. et al. 2004, *A&A*, 422, 177  
 Skinner, S.L., Güdel, M., Schmutz, W. & Stevens, I.R. 2001, *ApJ*, 558, L113  
 Skinner, S.L., Güdel M., Schmutz, W., & Zhekov, S.A., 2006, *Astrophys. Space Sci.*, 304, 97  
 Skinner S.L., Zhekov S.A., Güdel M., Schmutz W. & Sokal, K.R. 2010, *AJ*, 139, 825  
 Stevens, I.R., Blondin, J.M. & Pollock, A.M.T. 1992, *ApJ*, 386, 265  
 St-Louis, N., Moffat, A.F.J., Drissen, L., Bastien, P., & Robert, C. 1988, *ApJ*, 330, 286  
 St-Louis, N., Moffat, A.F.J., Lapointe, L., Efimov, Y.S., Shakhovskoy, N.M., Fox, G.K., & Pirola, V. 1993, *ApJ*, 410, 342  
 Sugawara, Y., Tsuboi, Y., & Maeda, Y. 2008, *A&A*, 490, 259  
 van der Hucht, K.A. 2001, *New Astronomy Rev.*, 45, 135  
 van der Hucht, K.A., Cassinelli, J.P., & Williams P.M. 1986, *A&A*, 168, 111  
 Vuong, M.H., Montmerle, T., Grosso, N., Geigelson, E.D., Verstraete, L., & Ozawa, H. 2005, *A&A*, 408, 581  
 Wojdowski, P.S. & Schulz, N.S. 2005, *ApJ*, 627, 953  
 Zhekov, S.A. 2007, *MNRAS*, 382, 886  
 Zhekov S.A., & Palla, F. 2007, *MNRAS*, 382, 1124  
 Zhekov, S.A., & Park, S. 2010a, *ApJ*, 709, L119  
 Zhekov, S.A., & Park, S. 2010b, *ApJ*, 721, 518  
 Zhekov S.A. & Skinner, S.L. 2000, *ApJ*, 538, 808

## APPENDIX A: DETAILS ON THE X-RAY DATA FOR WR46 AND WR79

### A1 WR46

One of the most interesting characteristics of WR46 is its variability established in the optical/UV (e.g., Marchenko et al. 2000 and the references therein). Since *XMM-Newton* is capable of providing optical/UV data simultaneously with the X-ray data, the corresponding WR46 observations allow to search for X-ray variability that may correlate with the one found in the optical/UV. Gosset et al. (2011a) and Hénault-Brunet et al. (2011) reported that such a correlation does exist (we note that Gosset et al. 2011a suggested that the X-ray variability is restricted only to the 0.2-0.5 keV energy range).

Adopting a recent version of the SAS software (§ 3), we extracted background-subtracted X-ray light curves (LC) from the reprocessed EPIC data. We also built UV LCs in the two filters (UVM2, UVW2) from the reprocessed data of the Optical Monitor used in these observations. For consistency with the UV data, the X-ray LCs are binned in 2000-second time intervals. Figure A1 presents the corresponding X-ray and UV LCs of WR46. We see that the variability pattern in WR46 is quite complex. Namely, the expected 0.329-day period is evident *only* in the UV filter UVW2. This is not the case for the other UV filter (UVM2) although these data are taken one after the other (see the left panel in the first row in Fig. A1). Such a behaviour is quite strange (or interesting) since the throughput curves for these filters overlap considerably (see Fig.88, § 3.5.5.1

in the *XMM-Newton* Users Handbook<sup>3</sup>). Similarly, the X-ray variability (if any) does not seem to be ‘identical’ in the EPIC detectors of a different kind: pn and MOS.

To quantify the variability pattern in WR46, we performed the following exercise that is indicative of whether the corresponding emission is variable. First, we fitted each LC with a constant (adopting  $\chi^2$  fitting). Second, excluding the two ‘extreme’ values, i.e. the maximum and minimum value, in each LC, we fitted the LC with a constant again. The result as a formal goodness of the fit is as follows. For the complete LC, the goodness of the fit for a constant emission is 0.0002 (UVM2), 0.0 (UMW2), 0.49 (X-ray, pn) and 0.99 (X-ray, MOS). In the case with the two extreme values excluded, the goodness of the fit is 0.24 (UVM2), 0.0 (UMW2), 0.87 (X-ray, pn) and 1.0 (X-ray, MOS). We note that excluding one or two data points from a sequence of measurements is not expected to change the global trend in a variability pattern of a physical quantity. Thus, we feel it is safe to conclude that only the UV emission of WR46 in the UVW2 filter of the optical monitor on-board *XMM-Newton* does show clear sign for *not* being constant. We believe that more X-ray and UV data, taken simultaneously, are needed to firmly establish whether the X-ray emission from WR46 is variable, and if it is, then on what timescale, on what luminosity scale and whether it correlates with the variability detected in other spectral domains (e.g., optical, UV).

### A2 WR79

The *XMM-Newton* observations of WR79 were analysed by Gosset et al. (2011b). But thanks to the *Chandra* superb spatial resolution, the ACIS-S images of WR79 reveal that there are two near-by sources within 6'' from WR79 (Fig. A2). We denote them as S1 (the northern source) and S2 (the southern source). The S1 coordinates are  $\alpha_{2000} = 16^h 54^m 19^s.41$ ,  $\delta_{2000} = -41^\circ 49' 08''.15$  and WR79 is the only object in SIMBAD within 5'' from S1 (radial distance of 4''.7). Source S1 is thus unidentified yet. The S2 coordinates are  $\alpha_{2000} = 16^h 54^m 19^s.44$ ,  $\delta_{2000} = -41^\circ 49' 16''.71$  (radial distance of 5''.9 to WR79) and the binary system CCDM J16543-4149D is the only object in SIMBAD within 2'' from S2 (radial distance of 1''.9). Source S2 is thus unidentified yet.

It is important to note that it is possible to extract a ‘net’ X-ray spectrum of WR79 from the *Chandra* data while only a total spectrum for all three sources, WR79, S1 and S2, can be obtained from the *XMM-Newton* data (Figs. A2 and A3). We see from Fig. A2 that S1 is definitely a variable source and Figure A3 illustrates that the X-ray emission from S1 and S2 may alter appreciably the X-ray emission from WR79 when the latter is observed with X-ray telescope having not very high spatial resolution. We note that the total number of counts from sources S1 and S2 amounts to 37-47% of that from WR79 as directly measured in the ACIS-S data of the two *Chandra* observations. Also, the X-ray emission of S1 and S2 is much softer compared to that of WR79 and if the total spectrum of these three sources is assigned to WR79 alone, then from analysis of such a ‘combined’ spectrum we may draw conclusions

<sup>3</sup> see Documents & Manuals on <http://xmm.esac.esa.int/>

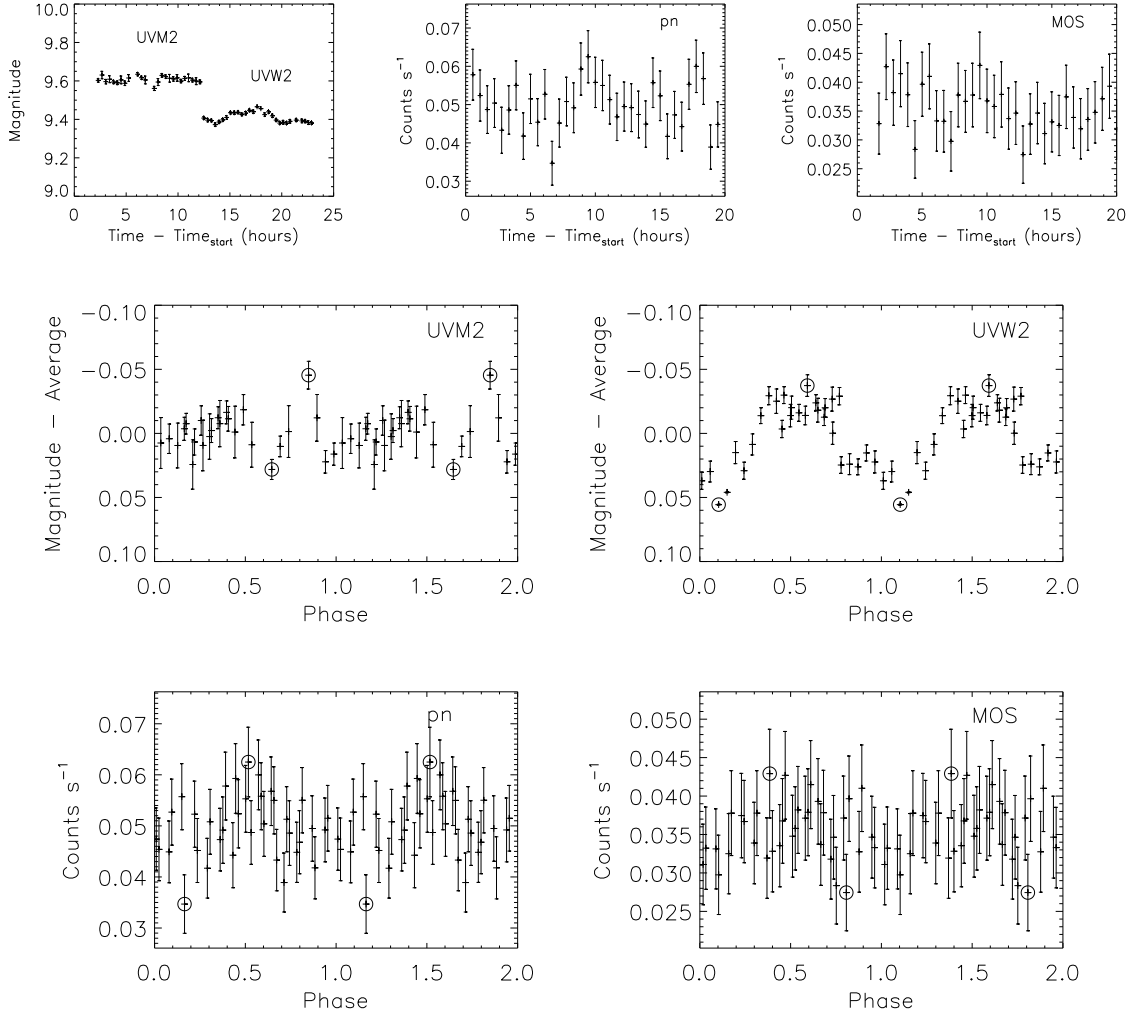


**Figure A1.** *XMM-Newton* light curves (LC) of WR46. *First row:* LCs as a function of observing time in two UV filters of the Optical Monitor (UVM2; UVM2) and in the (0.2 - 10 keV) energy range with the EPIC detectors (pn; MOS denotes the total emission from the two MOS detectors). *Middle and Bottom rows:* LCs folded with the orbital period; the values for period and zero-phase time are from Marchenko et al. (2000). Note that for graphical convenience the data points are plotted twice: the data for phase values (1.0-2.0) are the same as for phase values (0.0-1.0). Circles mark the maximum and minimum values in each LC. The X-ray LCs are background-subtracted.

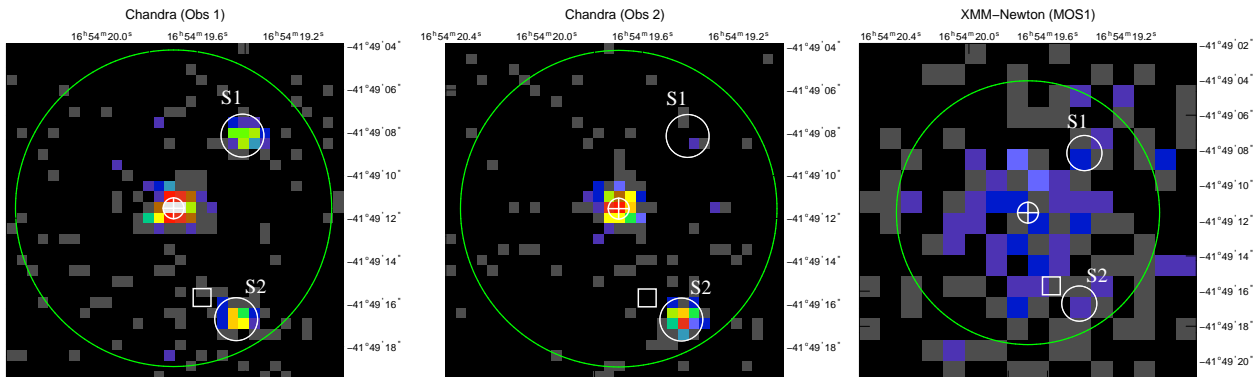


**Figure A2.** WR79 images: *Chandra* ACIS-S images for the two observations used in this study with ObsID 5372 (Obs 1) and 6291 (Obs 2), and an *XMM-Newton* MOS1 image (ObsID 0109490401). All images are centered at the optical position of WR79 (SIMBAD) marked by a circle with crosshairs. Two X-ray sources are seen in close distance from WR79: marked by a circle and denoted S1 and S2. A square marks the optical position of CCDM J16543-4149D (a binary system; SIMBAD). The green circle has a diameter of 15''.

about the X-ray characteristics (e.g., plasma temperature, X-ray absorptions, variability) that will not be quite correct. From all this, we can safely conclude that for the moment *Chandra* observations are the only ones that can provide us with valuable information on the X-ray emission from the WR+O binary WR79.

This paper has been typeset from a  $\text{\TeX}$ / $\text{\LaTeX}$  file prepared by the author.

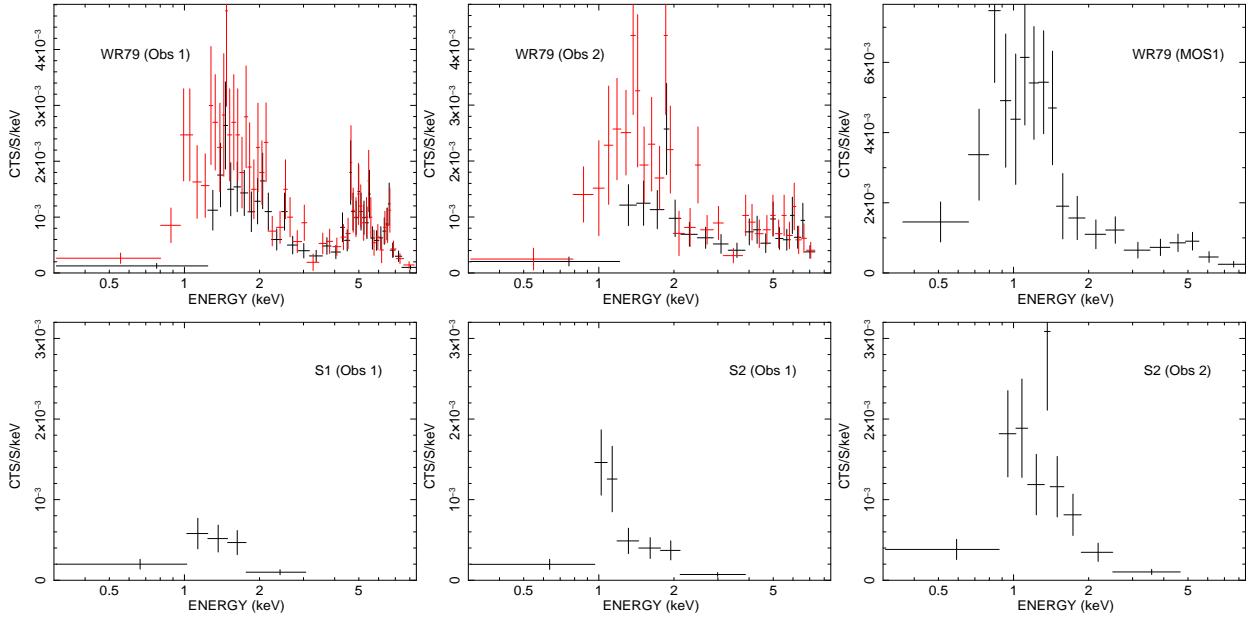


**Figure A3.** The background-subtracted spectra of the X-ray sources from Fig. A2. The WR79 spectra extracted from the *Chandra* ACIS-S data are shown in the first two panels of the upper row as those from the large extraction region having a diameter of 15 arcsec (shown in green in Fig. A2) are drawn in red while the spectra *only* of WR79 itself are given in black (they are the ones used in the current study, see Fig. 1). For comparison, the archive *XMM-Newton* MOS1 spectrum of WR79 is shown in the last panel of the upper row. The X-ray spectra of sources S1 and S2 (Fig. A2) are shown in the lower row. No spectrum of S1 from Obs 2 is presented since there are only 2 counts in it. All the spectra are re-binned to have a minimum 10 cts per bin.